SYNTHESIS REPORT

FOR PUBLICATION

CONTRACT No: ***BRE2.CT92.0180***

PROJECT No: BE-5248-92

TITLE: ***Development of a Decision Support System For Predicting Wear in Bulk and Sheet Forming Operations***

PROJECT
CO-O RDINATOR: ***Rockfield Software Limited***

PARTNERS:

Rockfield:	***Dr. Tony Crook***
UPC:	***Pro f.Eugenio Onate***
Matrix:	***Dr.Ing.Andreas Heege***
IPU:	***Prof. Tarras Wanheim***
DIMEG:	***Pro f.Paolo Bariani***
TECHINT:	***Dr.E. Dvorkin***
CANDEMAT:	***Mr.Gomez de Dies***

British Steel: Siib-contractor represented by Rockfield

REFERENCE PERIOD FROM. f-Dee-7995 to ***37-May-7996*** REPORT No: ***PIR9648***

STARTING DATE: ***1-Nov-1 992*** DURATION: 48 ***Months***

PROJECT FUNDED BY THE EUROPEAN COMMUNITY UNDER THE BRITE/EURAM PROGRAMME

Development of a Decision Support System for Predicting Wear in Bulk and Sheet Forming Operations

Project Number - BE-5248-92

Contract Number - BRE2-CT92-0180

SYNTHESIS REPORT

1-Dec-1992 - 30-Nov-1996

Report No. :/Predwear/PIR9648. DOC

Prepared by : T. Rodic Date : 20-Dec-1 996

Approved by : Date : _____

Issue :1.0 Date : 20-Dec-1 997

Partners

Dr. Tony Crook, *Rockfield Software Ltd.*, Innovation Centre, Swansea University, Singleton Park, Swansea, UK, SA2 8PP

Prof. Eugenio Onate, *Universidad Politecnica de Cataluna (UPC),* Gran Capitan s/n Modulo Cl, Campus Norte UPC, Barcelona 08034

Dr.*Ing.Andreas Heege* *Matrix Sa,* Vinas No 1, Ripoll, Spain

Prof. Tarras Wanheim *Institute for Product Development (IPU),* Lundtoftevej 100, 13 K-2800 Lyngby, Denmark

Prof. Paolo Bariani *University degli Studi di* Padova *(DIMEG),* Via Venezia, Padova, I-351 31, Italy

Dr. E. Dvorkin *Techint - Compagnia Tecnica Internazionale SpA,* Via Po, 24, I -00198 Roma

Mr.Gomez de Dies *Candemat Sa,* Maliano (Cantabria) 39600, Spain

British Steel, Sub-contractor represented by Rockfield

Project Officer

Dr Suzanne Becker

1. Abstract

The main objective of this project was to enhance available decision support systems used in the industrial design and optimisation practice in sheet and bulk metal forming to take into account the phenomena of wear. To meet this objective the research and development work has been performed in five main technical tasks dedicated to micromechanical modeling, laboratory testing, inverse analyses, finite element analyses and industrial applications. The decision support systems have been applied to the experiments! tests and also a number of industrial tests including production of car hood dies, blanking operations, cup drawing, double dogbone forging, crane hook forging and hot flat rolling.

2. Introduction

The phenomena related to wear have an important impact on the economy of the metal forming operations. The statistics show that wear is to within approximately 60-70% the dominating failure mechanism for hot forging dies and has therefore an important influence on the production costs of forged products.

The main objective of this project has been to develop experimental and numerical procedures to quantify of the effect of wear on the forming process. With this aim a multi-disiplinary consortium specializing in micromechanical and experimental research of wear, numerical analysis and tool and steel product manufacture. The tasks undertaken within the project are:

Task 1: *Micromechanical modeling*
Development and analysis of micromechanical models and formulation of governing equations

Task 2: *Laboratory testing of wear*
Design and setting up of laboratory tests and performing experiments

Task 3: *Inverse evacuation of wear parameters*
Estimation of permitted experimental errors, implementation of regularization techniques, inverse reconstruction of contact conditions and inverse identification of wear parameters

Task 4: *Finite element modeling and simulations*
Updating of numerical algorithms, direct numerical analysis of lab. tests and analyses of bulk and sheet forming operations

Task 5: *Industrial application*
Specification, setting up, and performing industrial tests and application of the decision support system

The products of this project are *decision support systems* based on *computer simulation* that furnish potential advances in the design and manufacturing of sheet stamping, blanking and forging processes by *reducing wear during forming operations,* hereby bringing about quantitative improvements in the competitive state of European die manufacturing enterprises. Additionally, the simulation tools enable a *more scientific approach to the design and manufacture process* allowing for the *optimisation of tool design and the production process* to both *extend fool life* and *reduce lead time and cost for new products.*

3. Technical Description

3.7 Task 1: Micromechanical Modeling

The fundamental understanding of friction has been improved via micromechanical studies of the dual asperity and third body abrasive friction models and a new formulation which accounts for variation of effective contact area and temperature has been developed. Within this section a dual asperity friction model, proposed by the Polish Academy of Sciences (ERBCIPACT940170), is described,

As usually the tool surface is smooth relative to the workpiece roughness, consider a dual asperity interaction assuming that workpiece asperities undergo flattening according to *smooth* fool-rough *workpiece* (ST/RW) model, whereas at the top of each workpiece asperity the local friction stress follows the *rough tool-smooth workpiece* (RT/SW) model prediction. Such dual asperity interaction was discussed by Wilson (1 991] who included also the effect of bulk straining on friction into his analysis,

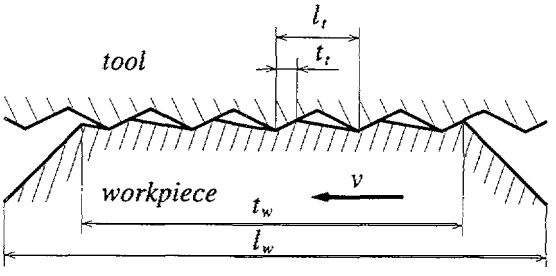

Figure 3.1-7 Dual asperity model. Typical dimensions of wedge asperities.

Referring to Figure 3.1-1 consider the tool-workpiece contact assuming workpiece wedge asperities of much larger size than that of tool asperities. Let the workpiece asperity length and the interaction length be denoted by l_w and t_w. Similarly, let the tool asperity length and the contact length be denoted by l_t and t_t. Let the non-dimensional fractional contact areas be denoted by α_w and α_t, thus

$$\alpha_w = \frac{t_w}{l_w}, \alpha_t = \frac{t_t}{l_t}, \alpha = \alpha_w \alpha_t \tag{1}$$

where α is the real effective contact area factor. The mean contact stresses at the workpiece asperity top $p_N^{(w)}, p_T^{(w)}$ are related to the global contact tractions p_N, p_T by the relations

$$p_N^{(w)} = \frac{p_N}{\alpha_w}, \qquad p_T^{(w)} = \frac{p_T}{\alpha_w}. \tag{2}$$

The limit abrasive friction condition $f_c^p = 0$ for RT/SW model can now be assumed to relate the local stresses $p_N^{(w)}, p_T^{(w)}$:

$$f_p^c = \left(p_N^{(w)}, p_T^{(w)}\right) = f_p^c = (\text{'\%. } > \text{'\%.}) = f_p^d = \left(p_N, p_T, \alpha_w\right) = 0 \tag{3}$$

This condition contains the contact state variable α_w associated with the workpiece asperity flattening mode. **In** the plane of total contact tractions p_N, p_T the Critics] friction condition 's represented by a set of limit friction surfaces $f_c^d = 0$ obtained for different values of α_w.

The intersection of limit friction surfaces f_l^d **=0** with flattening surfaces $f_s = 0$ provides the *critical state locus* $F_c(\bar{p}_N, \bar{p}_T)$ = O. Along the critical surface, both α_t and α_w vary. On the other hand, the limit friction surface $f_l^d = 0$ corresponds to fixed α_w reached after pressure preload.

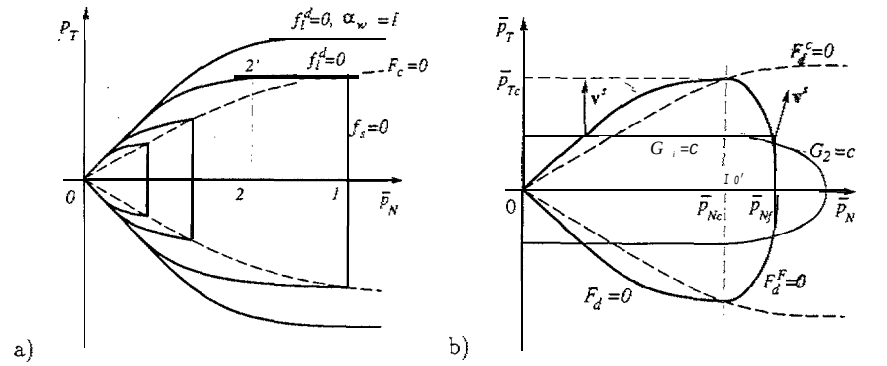

Figure 3. ***1-2 Dual asperity model: a) limit friction surfaces for different values of α_w; b) generalized model.***

Specification of model functions and parameters can be performed using the solutions for flattening and ploughing modes. The slip-line solutions of Wanheim ***et*** al. (1974) and Bay (1987) for the ST/RW model provide the relation between the effective contact area ***a = a*** $_w$ and contact pressure $\bar{p}_N$ with constant friction factor *m* as a parameter: $\alpha_w = g_2(\bar{p}_N, m)$.

The ploughing mode was analyzed by numerous researchers, Avitzur and Nakamura (1986), Wilson and Sheu (1988,1991). The results of those micromechanical models can be approximated by analytical relations and used in the model of dual asperity interaction. Moreover, the friction stress can be decomposed into adhesive and ploughing portions, $\bar{p}_T = \bar{p}_T^a + \bar{p}_T^p$.

The constitutive equations following from ST/RW and RT/SW models are expressed in terms of non-dimensional contact tractions $\bar{p}_N = p_N / k$, $\bar{p}_T = \tau_T / k$ where *k* is the shear yield stress of the workpiece. In the general case, *k* depends on the temperature of the workpiece surface. Thus, the model accounts for surface temperature changes. Those effects can be important in hot working processes, in which significant temperature changes can occur. Similarly, the variation of *k* due to workpiece material strain hardening can be accounted for.

A more general model can be formulated by assuming that the condition of asperity flattening depends on both normal and tangential contact stresses. Assuming the compaction surface in a form of rotational ellipsoid, Figure 3.1-2b,

$$f_s^d = (\bar{p}_N, \bar{\boldsymbol{p}}_T, \alpha_w) = \frac{(\bar{p}_N + \bar{p}_{N_c})^2}{(\bar{p}_{N_f} + \bar{p}_{N_c})^2} + \frac{\|\bar{\boldsymbol{p}}_T\|^2}{(p_{T_c})^2} - 1 = 0 \quad \text{for} \quad \bar{p}_N > \bar{p}_{N_c}, \tag{4}$$

where $\bar{p}_{N_c}$ specifies the ellipsoid centre, $\bar{p}_{T_c}$ and $\bar{p}_{N_f} - \bar{p}_{N_c}$, are its lengths of semi-axes. The non-associated slip rule is governed by the slip potential $G = (\bar{p}_N, \bar{\boldsymbol{p}}_T, \alpha_w)$, composed of a cylindrical surface $G_1 = \|\bar{\boldsymbol{p}}_T\|^2 = \text{const.}$, and a rotational semi-ellipsoid $G_2 = \text{const.}$ The slip

potential G_2 corresponds to the compaction surface f_s^d = **O,** eqn (4). Both semi-ellipsoids have common centres, but different ratio of semi-axes.

3.2 Task 2: Laboratory *Testing of Wear*

In laboratory *simulative tests,* model **test** specimens rather than actual tribocomponents are tested under practice-oriented operating conditions. The test configuration must have sufficiently similar structural, operational and interaction parameters to the industrial hot and warm forging or sheet forming tribosystems to be analysed. Therefore, particular care has been taken in reproducing the physical/chemical nature of the model test specimens and sliding velocity, stresses and temperature at workpiece-tool interface. On this basis, new double combined piercing and BUT sheet forming experimental tests have been developed.

3.2. 1 Double Piercing Tesf

The double piercing test has been performed by DIMEG and has the following geometry

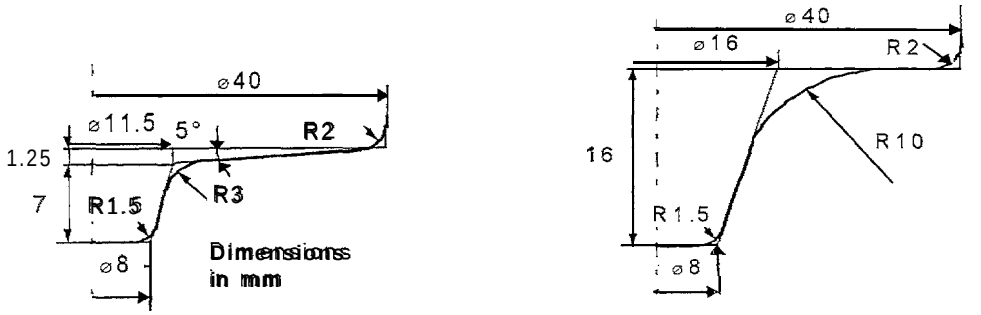

Fig.3.2-1 Profiles of the two pairs of test punches.

The geometries exhibit three tribological features

. *The* cone *top and* edge - the tool surface can reach high temperatures and pressures so that thermal fatigue and plastic deformation being the main failure mechanisms.
. *The* cone *flank* - the contact pressure is relatively low throughout the process but the sliding length is long so that a sharp peak of the wear can develop.
• *The* ***fiat*** *surface* ***surrounding*** *the cone.* - the workpiece material tends to separate from the punch near the cone whilst on the flat surface a rather high and uniform potential wear develops, mainly with long piercing strokes.

3.2.2 The BUT Strip Drawing Test

The BUT drawing test is a new test proposed by IPU to provide a more realistic stress and strain field within the sheet than the more commonly used tribological systems.

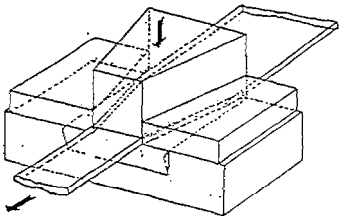

Figure 3.2-2 ***The BUT test.***

The BUT test provides a much closer agreement with σ_x rising from zero at the entrance to the converging dies to a finite level corresponding to σ_r in deep drawing, σ_y is constant and relatively

low thoughout the section and rises on the die radius, and σ_z starts relatively high and drops towards a minimum. The BUT test has been incorporated into a new sheet metal tribotester and used for wear evaluation within the scope of the project.

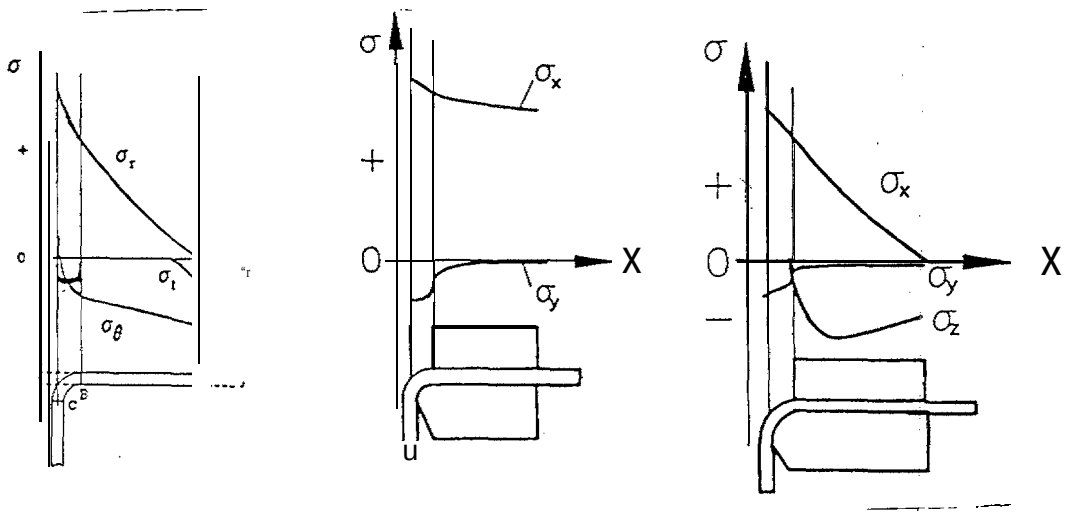

a)* Drawing *of a cup ***b) Standard test*** ***c) BUT test***

Figure 3.2-2 Comparison between Standard and BUT test.

3.3 Task 3: inverse Evaluation of Wear Parameters

Inverse methods provide an efficient link between numerical analysis and laboratory experiment. This is presented in Figure 3.3-1 where the function of inverse shell is illustrated. Consider a laboratory test where a number of quantities such as force, displacements, strains and temperatures are measured. Consider also that the test is simulated by numerical analysis. In order to minimise the difference between the numerical results and experimental measurements the inverse analysis shell can be applied. The shell is implemented as a computational loop over the finite element solver in which model parameters contained in the input data are automatically updated until the numerical results match the experimental measurements in a least square sense. The shell can be applied to evaluate material properties and frictional constants as well as to reconstruct thermomechanical processing conditions. The advantage of the inverse approach is that it permits evaluation of desired quantities from indirect measurements even if stress/strain fields are not uniform during experiments.

The inverse analysis shell developed in this project has a number of facilities which enable solution a wide variety of mechanical, thermal and coupled inverse problems (see e.g. Rodic *et al.* 1995). This includes modules for definition of the objective function, control of the minimisation procedure, automatic updating of model parameters, sensitivity evacuation, regularization procedure, etc.

3.3.7 *Numerical Sensitivity Approximation*

Since forming operations are non-linear, transient and path dependent it is difficult to evaluate implicit terms of response functional. Therefore sensitivity studies are often performed by an approximation of the differentiation of the general response functional numerically. This can be done by perturbing parameters ϕ_i one by one and rerunning complete non-linear finite element analysis for each perturbed parameter. The technique is simple to implement but can be computationally very expensive, especially if the number of design parameters is large. Further drawback of this approach is that it is prone to round-off and truncation errors.

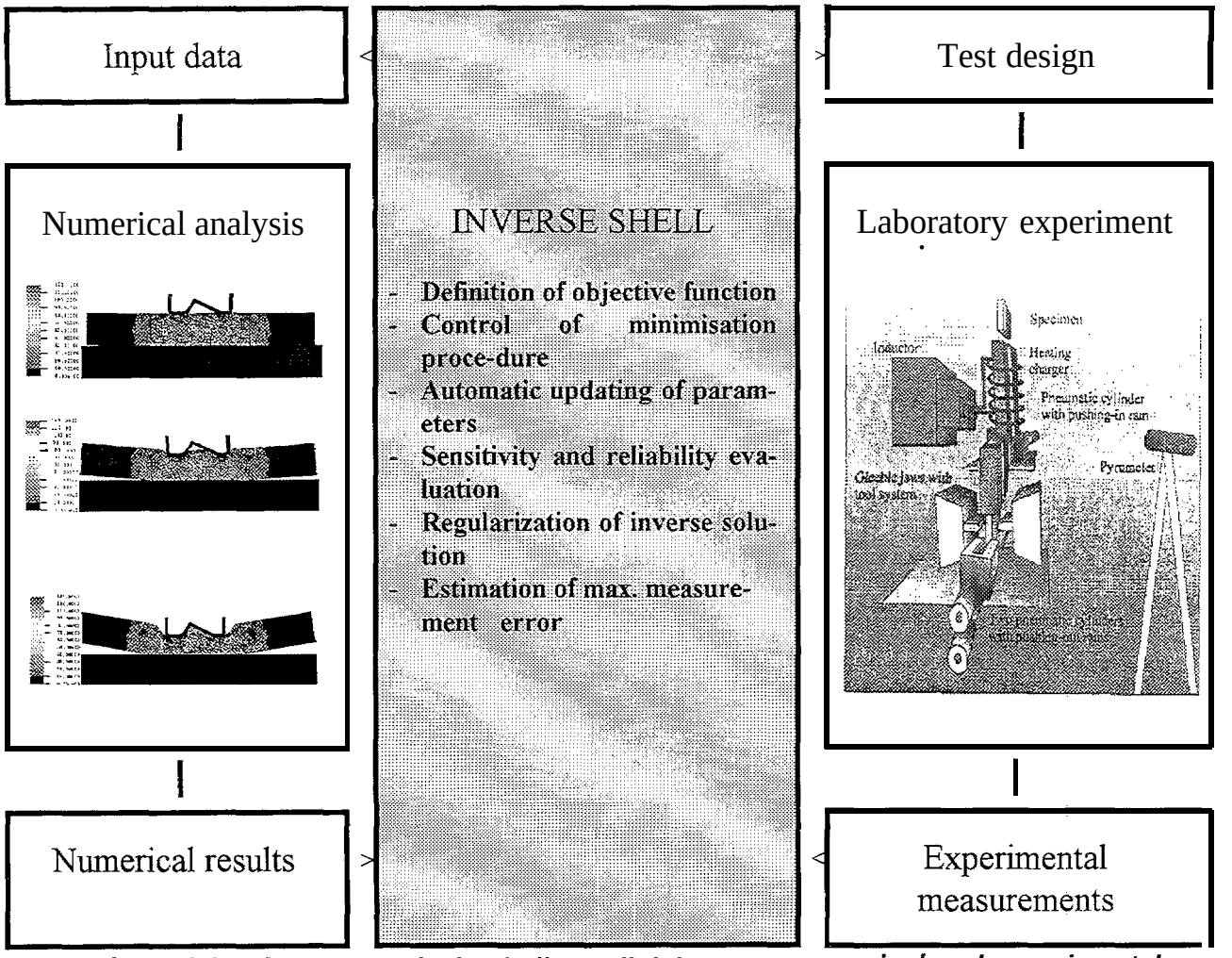

Figure 3.3-7. Inverse analysis shell as a link between numerical and experimental investigations

Methods used are the *direct differentiation* where consistent tangent operator from the FE analysis is employed, and the *adjoint sensitivity* method where adjoint sensitivities are obtained via the Lagrange multiplier method. The adjoint method requires the solution of one adjoint problem for each response functional *F.*

3.3.2 *Comments on Sensitivity Evaluation*

Analytical techniques to evaluate sensitivities such as direct differentiation and adjoint method are computationally much more efficient than numerical approaches. Consider for exampie a sensitivity study for a model with *N* parameters. if a numerical sensitivity evaluation is employed then *N+1* direct finite element analyses need to be performed to evaiuate sensitivities with respect to each parameter. The analytical approaches on the other hand add oniy a small fraction of the overail computational cost to the solution of a single direct problem. Note that even for a complex non-linear, coupled and transient problem the sensitivity evacuation is reduced to the solution of iinear systems depending on the chosen approach.

in this project inverse approach was applied to evaluate hardening parameters in plasticity from the tension testwhere heat transfer coefficient between the tool and the workpiece in hot forging and wear parameters from laboratory were obtained.

3.4 Task 4: Finite Element Modeling and Simulations

[n the context of finite element analysis of path dependent problems, the load path is followed incrementally and a numerical approximation to the material constitutive law is needed to update stresses as well as the internal variables of the problem within each increment or time step. Then, given the values of the variables On, $\mathbf{q}_n$ at the beginning of a generic step t_n, t_{n+1} an algorithm for integration of the evolution equations is required to obtain the updated values $\sigma_{n+1}, \mathbf{q}_{n+1}$ at the end of the step. For convenience, the operations on the kinematic level are separated from the operations at the constitutive level and in both cases the stress update procedure is specifically designed to enable small strains elastic predictor-plastic corrector constitutive models using backward *Euler* time integration and *Newton-Raphson iteration* to be used. Therefore the constitutive model is independent of the global solution algorithm.

In *implicit formulation*, due to its suitability for the computational treatment of finite strain elasto-plasticity, the hypothesis of multiplicative decomposition of the deformation gradient is currently widely employed in the computational mechanics. The implementation uses the constitutive model defined using a quadratic strain energy function and the logarithmic strains as strain meassure.

The number of operations required for the implicit stress update algorithm render it undesirable for very large *explicit simulations*. Therefore, in these cases the stress update is performed using the Green-Naghdi stress rate as the constitutive relationship is formulated in a material system in terms of pure stretches enabling an identical constitutive model to the implicit algorithm and the strain rate is evaluated at the mid-step providing thus a second order approximation to the log strain, Resulting number of operations required to update the stress is very small.

From point of view of finite element technology, the use of *low order* cinematically based finite elements if preferable for both implict and explicit analysis. However, it is well known that the performance of these elements is extremely poor near the incompressible limit. Problems of forming simulations under plastic dominant deformations and the assumption of isochoric plastic flow are included in this class. For implicit approach, the *F-Bar* formulation proposed by de Souza Neto et al. [8] has been utilised. Briefly, the elements are based on the concept of multiplicative deviatoric/volumetric split in conjunction with the replacement of the compatible deformation gradient field with an assumed modified counterpart. The advantages of the algorithm are independency of the resulting formulation on the material model and maintenance of the strain driven format of the algorithms for integration of inelastic constitutive. [n expiicit formulation, low order one point quadrature elements with an *hourglass* control are widely used. The relatively recent formulation proposed by Belytschko *et* al. [4] was utilised in this work as it has been found to be more effective in eliminating hourglassing than earlier formulations.

In our work error indicators based on the *plastic dissipation functional* and the rate *plastic work [6]* have been found to be the most appropriate error estimator for metal forming processes. For forging problems the error estimator is also supplemented by element distortion checking, whereby several measures of distortion, e.g. corner angle and element slenderness, may also trigger re-meshing. Then, the mesh refinement procedure is constructed with the objective of minimizing the local error. This procedure is subject to additional optional constraints, e.g. minimum and maximum element sizes, to ensure that the solution cost remains viable.

An unstructured meshing approach is used for the mesh generation and subsequent mesh adaptation. The algorithm employed is based on the *Delaunay triangulation* **for 2D problems and** *avancing front technique* **for** 3D **problems. The methods have been extended to quadrilateral elements to enable employment of the low order elements described above.**

After creating a new mesh, the transfer of displacement, velocity and history-dependent **variables from the** old **mesh to a new mesh is required. Several important aspects of the transfer operation have** to **be addressed:** *Consistency with the constitutive equations; Requirement of equilibrium (which is fundamental for implicit FE simulation); Compatibility of the history--dependent in ternal variables transfer with the displacement field on the new mesh; Compatibility with evolving boundary conditions; Minimisation of the numerical diffusion of transferred state fields.* **The transfer process is similar for both the implicit and explicit algorithms in that the transfer operators are identical.**

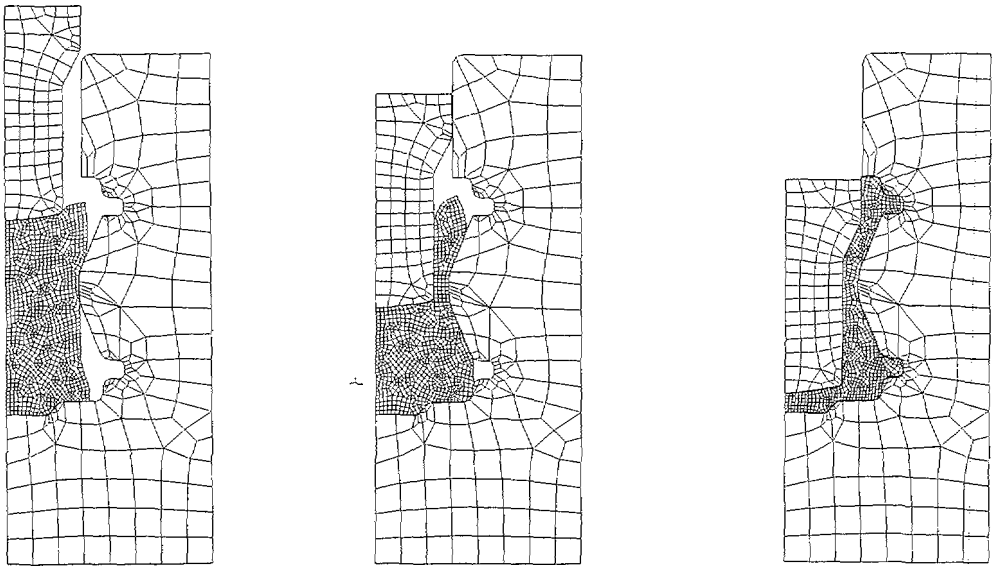

Figure* 3.4-1 *Complex axisymmetric aluminium forging.

4. Application of Decision Support System

The developed *Decision* Support *System* has been applied both to the experimental and industrial tests.

4. 1 Experimental Tests

4. 1.1 Double Piercing Test

The wear test is carried out on a Gleeble 2000 system equipped with the special testing device and integrated with an external electrical furnace. The wear test cycle consists of the following four stages:

Stage A: Heating.
Stage B: Lubrication and loading.
Stage C: De formation.
Stage D: Unloading.

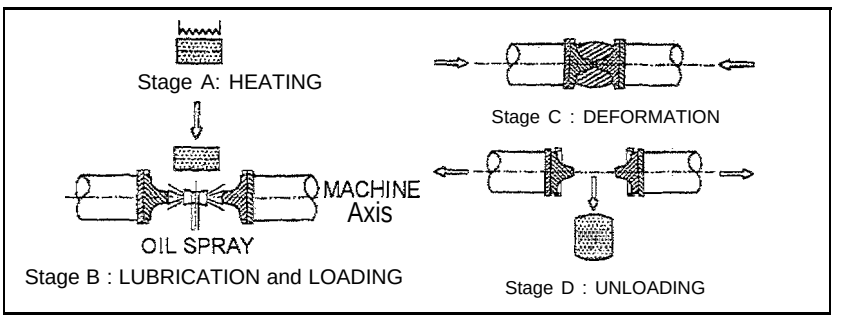

Measured wear has been compared with its numerical estimation based on the Archard's wear model [3]. In this model, abrasive wear is a function of normal pressure P_i, local sliding velocity v_i and tool hardness H_i, as follows

$$Wear_i = K \int \frac{P_i v_i}{H_i} dt$$

The following operationa! parameters have been measured:

- *Wear Distribution* -evaluated using a Zeiss UMM 550 coordinate measuring machine with *Holos* software.
- *Tool* Hardness. The hot hardness of the punch was evaluated in the temperature range
- *Pressure and Sliding Velocity*. the distributions of pressure and sliding velocity at the punch-specimen interface have been measured in larger scale tests using layered wax models.

An inverse numerical technique was used to improve FEM. prediction of the thermal field in the wear test through evaluation of the heat transfer coefficient [4]. A typical test configuration is:

- specimen and punch materials are DIN Ck40 and DIN X38CrMoV51 respectively
- the two punches are preheated at 300 °C by embedded electrical heaters,
- the temperature of specimens before starting deformation is 1100 'C,
- the lubricant (Sinol CS90) is sprayed on active surface of two punches before each stroke

The surface of the punch has been digitised after each 50 strokes. Fig. 4.2-5 show an isometric representation of the worn surface of one of the two punches after 50 and 250 strokes respectively. According to the classification of the tribological features, two main areas can be recognised on the worn surface:

- *the cone top and edge surfaces,* where thermal fatigue and plastic deformation are the main wear mechanisms, and

• *the* cone *flank* and *bottom* surfaces, where abrasive wear prevails.

At the cone flank and bottom surfaces, three adjacent zones are shown in Fig. 4.1-1, where different operating conditions take place and different wear levels are measured:

. Area A, where plastification occurs and a partial lose of contact reduces wear
. Area B, where less plastification occurs and no lose of contact results in increased wear.
• Area C, where no plastification is present, as well as no lose of contact.

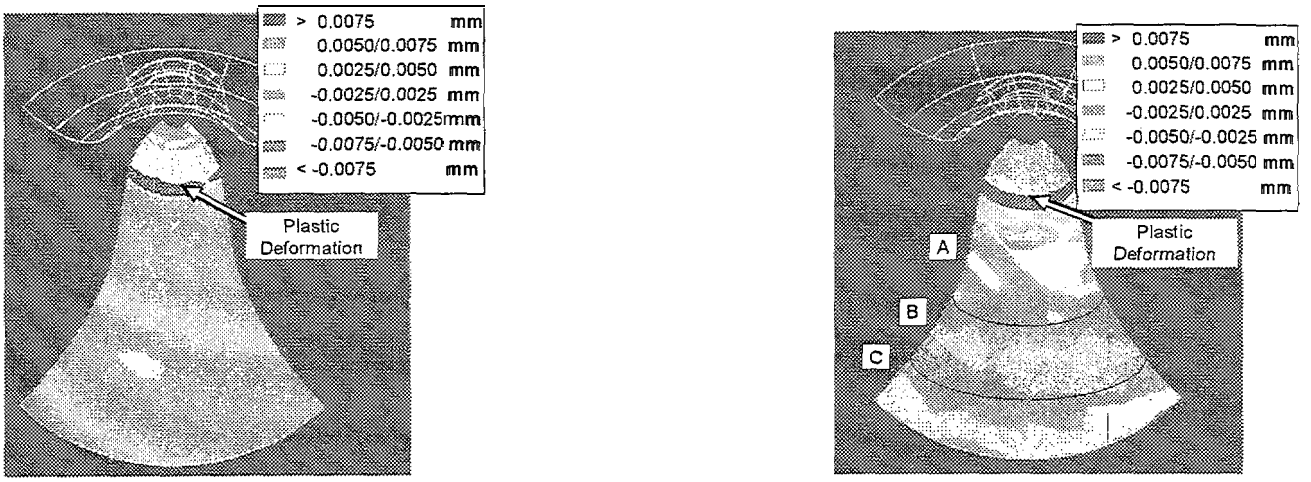

Fig.4.1-1 Digitised punch *surface* ***after*** 50 *and* ***after*** *250 strokes.*

In following table, measured (MW) and calculated (ARCH) values of the wear are compared. The calculated values have been obtained by using the Archard's model (eq. (1)), where $K=1$, P and v are predicted by numerical analysis and H is the hot hardness of the punch material.

Area	R [mm]	mess. wear [μm]	Temp [°C]	pred. wear/K	K
A	**7.14**	**36.00**	**420**	**0.963**	**37.399**
	7.33	45.33	425	1.079	42.010
	7.78	55.60	442	1.114	49.897
B	**8.42**	**80.00**	**424**	**1.087**	**73.567**
	9.27	**76.00**	**424**	**1.015**	**74.908**
C	**10.27**	**69.00**	**415**	**0.656**	**105.196**
	11.41	47.17	403	0.489	116.944

4. *?.2 BUT Sheet Drawing Simulator*

4. *1.2.1 Numerical Simulation*

A numerical model incorporating a wear estimate has been developed by UPC, to be able to predict tool wear profiles in forming operations. In the BUT test a strip is drawn through a blank holder and a die, following a rounded die corner. The dimensions of the blank holder are 125 mm long **and 4** mm high. The die has a corner radius of 5 mm. The initial thickness of the sheet is 1 mm, A finite element mesh of 327 and 69 4-node continuum elements using a mixed formulation has been used in the discretization of the sheet and the blank holder, respectively. Sheet discretization has been performed by using 3 rows of elements through the thickness. The

die has been modelled as a rigid body using 109 elements. The blank holder force is and the test is carried out for a slide length of 30 mm

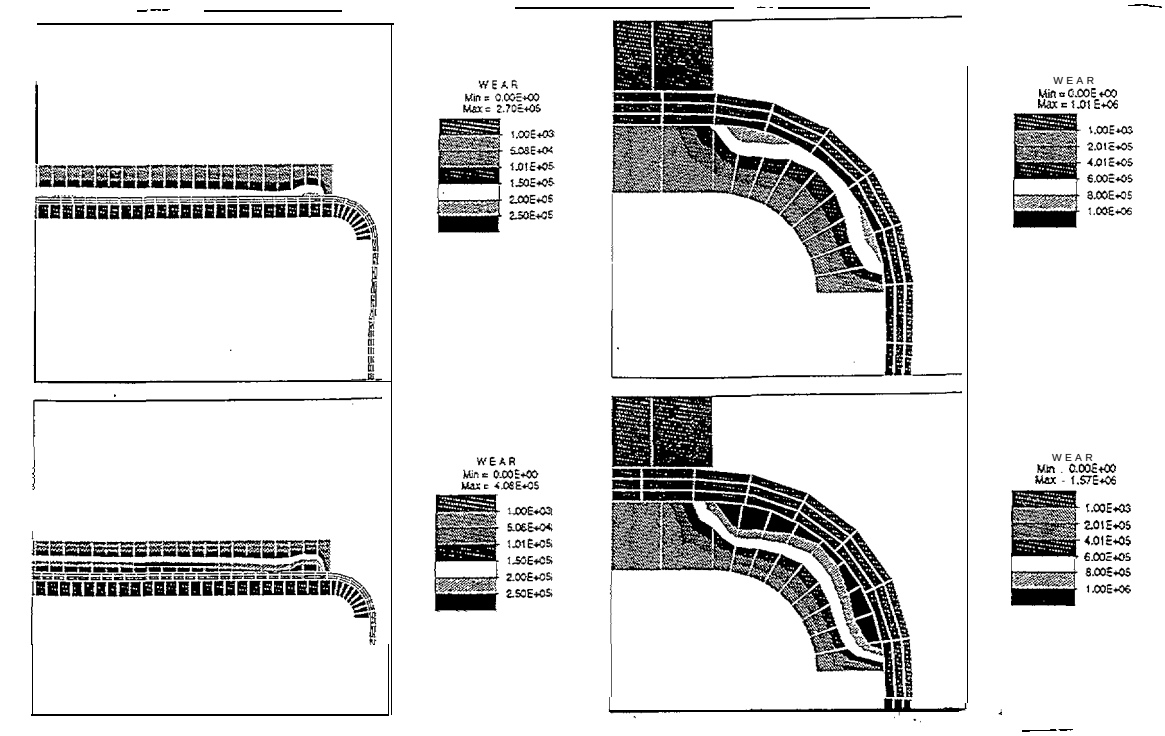

Figure** 4.1-2 **Wear profiles on the blankholder and tool radius.

Figures 4.1-2 show the wear profiles obtained for the BUT test on the blankholder and the die corner radius, respectively, at different stages of the drawing process. It is clear, that maximum wear of the blank holder surface is expected in the area near the die corner radius. On the other hand, the wear profile obtained on the die corner radius surface shows two peaks. These phenomena were also shown in the experimental results obtained by IPU.

4.2 Industrial Tests

4.2.1 Optimisation of Die Radii in Symmetrical Deep Drawing

When manufacturing cylindrical cans by deep drawing the geometrical opertunities for optimisation of the die, with regard to wear, is normally rather limited as the die geometry is normally dictated by the shape of the final product. [n this application, it is described how the tool life in deep drawing can be extended by more than 100% by small changes in die radii that are within acceptable tolerances for most products. The optimisation process was performed by IPU, specialists in experimental measurements, using the finite element progamme ELFEN, enhanced by Rockfield Software within the project.

Modification of the die radius

Figure 4.2-1 shows the effect of using this method with radii of 3, 5 and 10 mm for the cup drawing example.

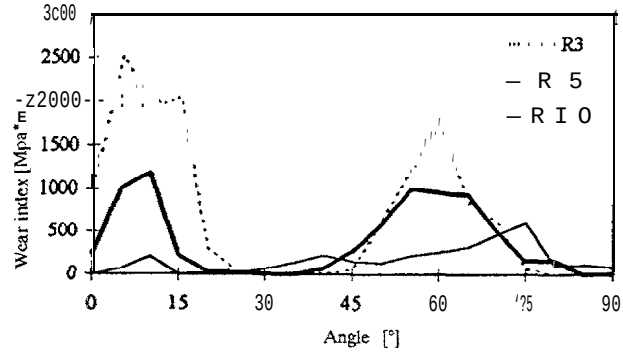

Figure 4.2-7. Accumulated Wear Index for Radii 3, 5, 10 mm.

R can be seen that the wear is decreasing with increasing die radius. However, it is also apparent that the wear index is not uniform over the die radius, but concentrated at approximately 10° and 60-70° around the die radius. This is due to a non-uniform pressure distribution around the die radius.

Small Die Curve Changes (SDCC)

A more uniform pressure distribution may be obtained on the drawing die radius by changing the geometry of the curve with which it is defined: The ensure that the modified curve is acceptable, in terms of the geometry of the final product, the allowable parametric changes are limited as shown in figure 4,2-2.

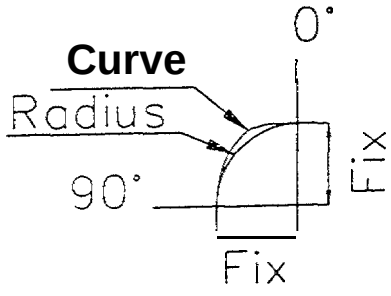

Figure 4.2-2. Schematic representation of the allowable changes SDCC.

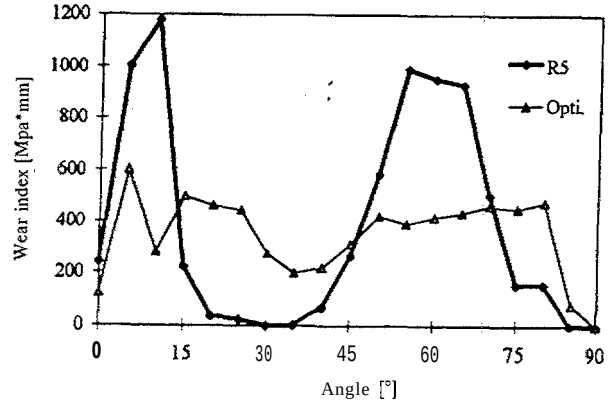

Figure 4.2-.3. Wear index for a 5mm radius and an optimized radius.

The optimisation process is performed as follows:

1. Add material to the locations on the curve where the wear index is a minimum i.e. ensuring that a larger share of the load is carried at these locations
2. Perform a simulation using the decision support system
3. Evaluate the sensitivities for the geometrical changes
4. Check whether further geometrical changes are required. If true return to 1

The resulting curve , after applying extra material to a 5 mm radius, exhibits uniform wear distribution as shown in figure 4.2-3.

It may be concluded that the decision support system ELFEN has been used to optimise the industrial cup drawing process. The modifications required are sufficiently minor to be acceptable with respect to the serviceability of the final product. The modified design is currently being used in the production of the industrial part.

4.2.2 *Wear of Rolls in a Flat Steel Hot Rolling Line*

[n this section, the phenomenon of rolls wear in hot-rolling of flat steel products is studied. An Archard's adhesive/abrasive wear model and the results are compared with industrial data obtained from SIDERAR (San Nicolás, Argentina), a steal -mill controlled by TECHINT.

In Fig. 4.2-4 the hot-rolling line for flat steel products operating in SIDERAR is schematized.

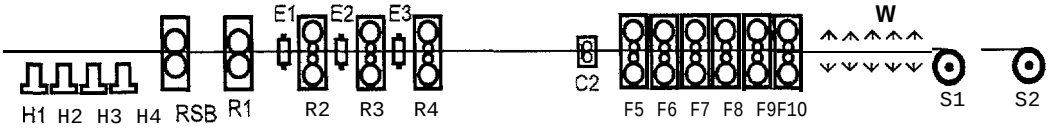

Figure 4.2-4 ***Layout of hot strip mill***

Here, following notation is used: RSB: roughing scale breaker; Rl, **R2, R3, R4:** roughing stands; El, E2, E3: edger rolls; Hl, H2, H3, **H4:** re-heating furnaces; C2: crop shear; F5, F6, F7, F8, F9, F1 O: finishing stands; W: water cooling; S1, S2: sheet toilers.

It is important to remark that, regarding the contact/friction stresses involved in the process, it is possible to divide the rolling stands into two types using the parameter H [5]:

$$H = \frac{R}{t_{in}} \left| \frac{t_{in} - t_{out}}{t_{in}} \right| \tag{5}$$

where ***R is*** rolls radius, t_{in} is thickness of the plate at the stand entrance, and t_{out} is thickness of the plate at the stand exit. Li and Kobayashi [4] stated that for $H < 3$ (*type 1* stand) indicates a double-peak type of contact pressure distribution. In this case the deformation pattern is more inhomogeneous. For $H > 3$ (*type* 2 stand) indicates a friction-hill type of contact pressure distribution. [n this case the deformation pattern is more homogeneous.

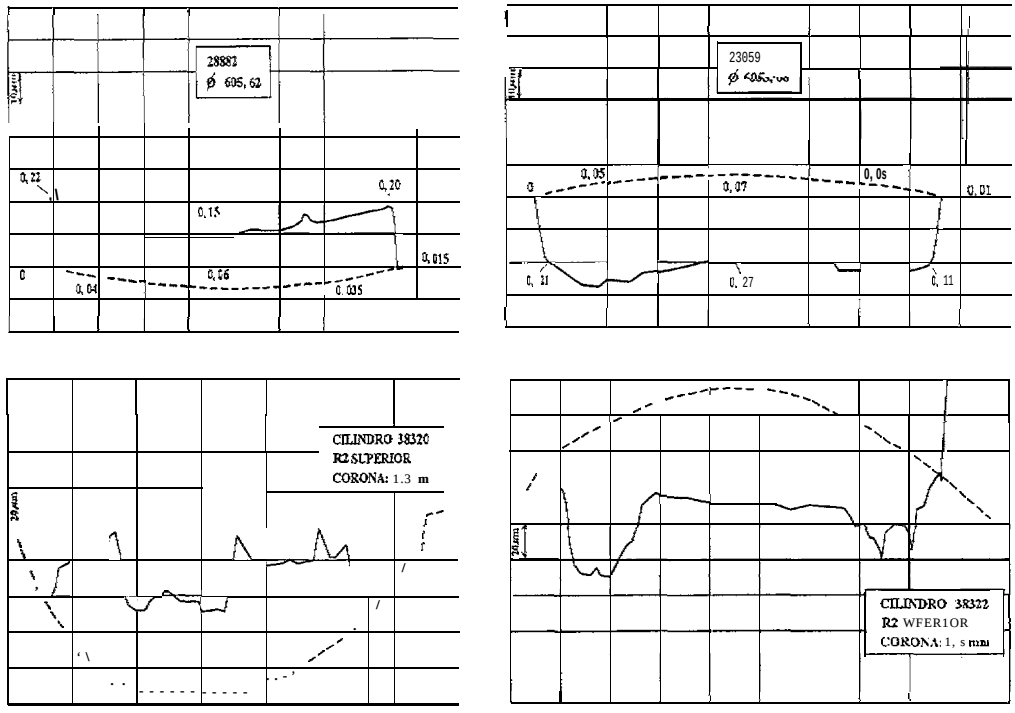

Figure 4.2-5 Typical profiles corresponding to new and worn rolls.

Archard's model for rolling applications can be stated as [4]:

$$\Delta D = k \frac{2}{\pi} \frac{1}{(HV)D} \sum_{i=1}^{N} \frac{F_i L_i}{W_i} \tag{6}$$

where ΔD is diametral roll wear [mm] in a round, HV is roll Vickers hardness [Kg/mm2], D is roll diameter [mm], N is number of coils processed in the round, F_i is separating force for the i-th coil [Kg], L_i is length, at the stand exit, of the strip corresponding to the i-th coil [mm], W_i is width, at the stand exit, of the strip corresponding to the i-th coil [mm].

In order to predict a-priori the wear for each stand it is necessary to:

(i) Determine for each stand/rolls material a reliable value of "k" using available industrial data-bases.
(ii) Determine the separating force using finite element models.
(iii) Determine the wear using Eqn. (5).

This method of wear determination uses Archard's wear law and assumes that the separating force is uniformly distributed across the rolls (e.g. as predicted by a 2D finite element model). We found that the results were in good agreement with experimental determinations of wear in the case of a finishing stand but that agreement, in the case of a roughing stand, was from mediocre to bad. However, in a roughing stand the assumption of uniform separating force across the rolls has to be improved.

The R4 stand was analysed using a 3D finite element model that incorporates the elastic flexibility of the work and back-up rolls and obtained the separating force distribution shown in Fig. 4.2-6. It is clear, that:

- The wear pattern of the finishing stand is approx. constant across the roll (Fig. .4.2-5 (c)).
- The wear pattern of the roughing stand rolls presents increased worn zones where the plate edges contact the rolls (Figs. 4.2-5.a and b).
- The separating forces present a peak at the plate edges {Fig. 4.2-6) and this explains the increased worn zones at the plate edges and the poor results obtained when a uniform wear is assumed.

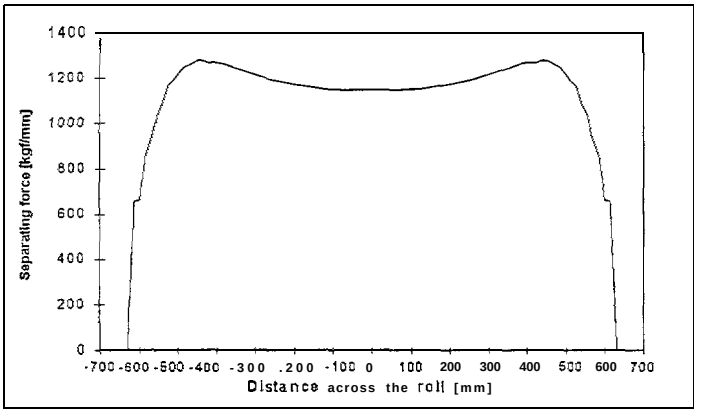

Figure 4.2-6 ***Separating forces at the R4 stand, predicted using a 3D finite element model.***

The conclusions that may be drawn from the study are:-

In order to produce an accurate prediction of rolls wear in a stand a system composed by a FEM model of the stand, followed by Archard's adhesive/abrasive wear model can be used provided that:

- The FEM model incorporates properly determined friction coefficients, steel material properties and stand temperatures.
- Archard's law is used with constants determined using extended data bases with rolls properly separated into upper an lower positions.

Another possible improvements are:

- The use of 3D models of the stand that although may be less efficient regarding computational resources, may increase the accuracy of the prediction.
- The use of an improved version of Archard's model that incorporates the fact that on the rolls $\sigma_{nn} > \sigma_y$, and the effect of thermal fatigue on the rolls surface.

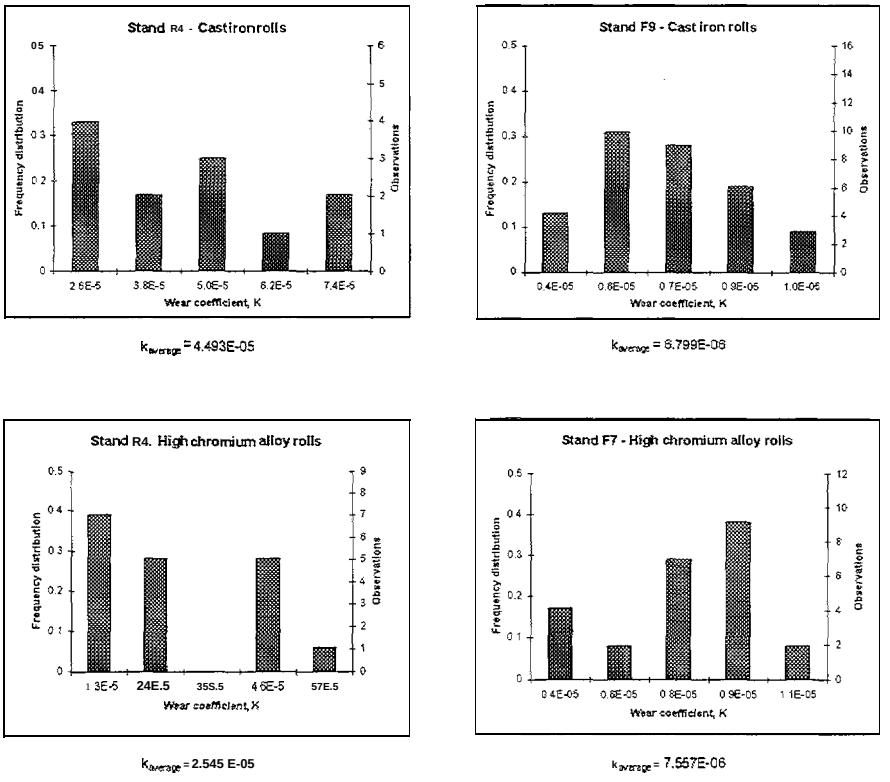

Figure 4.2.2-2 Wear profile on roller surface.

5. Conclusions

The key achievements of the project are:-

. The fundamental understanding of friction has been improved via micromechanical studies of the dual asperity and third body abrasive friction models and a new formulation which accounts for variation of effective contact area and temperature has been developed. It has been shown that wear rate is determined by frictional dissipation rate instead of the term involving the normal pressure as in the classical Archard law and a generalised wear model has been developed which allows treatment of different friction and wear mechanisms coexisting in real contact conditions.

- New designs of double piercing test, flat die test, bending under tension with flat dies, bending under tension with wedge-shaped dies and draw bead simulator have been developed.

- An efficient link between experimental measurements and computer simulations has been established via an inverse shell. The inverse analyses have been applied to evaluation of hardening parameters in plasticity, estimation of heat transfer coefficients and thermomechanical contact conditions.

- *Decision support* systems based on the finite element method have been developed that are capable of simulating forming processes that include large strains and deformations, frictional contact between workpiece and tool, complex constitutive relations and thermomechanical coupling. Adaptive remeshing techniques and efficient pre- and post-processing have also been provided.

. The decision support systems have been applied to the experimental tests and also a number of industrial tests including:-

(i) production of car hood dies
(ii) blanking operations
(iii) cup drawing
(iv) double dogbone forging
(v) crane hook forging
(vi) hot flat rolling

6. Acknowledgements

Additional contributions to this initiative originate from the Copernicus project ERBCIPACT940170 which was concerned with the development of decision support system for predicting wear of hot and warm forging dies and from Dr. Andrea Lovato who was a fellowship holder at IPU within the scope of Brite/Euram Action II.

7. References

[1] Avitzur, B. and Nakamura Y. (1986), Analytical determination of friction resistance as a function of normal load and geometry of surface irregularities, *Wear*, 107, 367–383.

[2] Bariani, P.F. et al., 1996, Determination of the Heat Transfer Coefficient in the Die-Billet Zone for Nonisothermal Upset Forging Conditions, AMST '96, p. 363-370.

[3] Bay, N. (1987), Friction stress and normal stress in bulk metal forming processes *J. Mech. Working Technol.*, **14**, 203–224.

[4] T, Belytschko, L.P. Bindeman (1991), Assumed strain stabilisation of the 4-node quadrilateral with l-point quadrature for nonlinear problems, *Comp. Meth. Appl. Mech. Engng.*, 88, 311-340.

[5] Li, G. and Kobayashi, S. (1982), Rigid-plastic finite element analysis of plane strain rolling, *J. of Engng. for Industry, 104, 55-63.*

[6] Peric, D., Yu, J. and Owen, D.R.J. (1994), On error estimates and adaptivity in elasto-plastic solids: applications to the numerical simulation of strain localisation in classical and Cosserat continua, *Int. J. Num. Meth. Engng, 37, 1351-1379.*

[7] Rodic, T., Gresovnik, I. and Owen, D.R.J. (1995), Application of error minimisation concept to estimation of hardening parameters in the tension test, in *Proceedings of the Forth* International Conference *on Computational Plasticity and Applications, 779-786.*

[8] de Souza Neto, E. A., Peric, Dj., Dutko, M. and Owen, D.R.J. (1996), Design of simple low order finite element for large strain analysis of nearly incompressible solids, *Int. J. So/ids Struct. 33, 3277-3296*

[9] Wanheim, T., Bay, N. and Petersen, A.S. (1974), A theoretically determined model for friction in metal working processes, *Wear, 28, 251-258.*

[10] Wilson, W.R.D. and Sheu, S., (1988), Real area of contact and boundary friction in metal forming, *Int. J. Mech. Sci.*, 30, 475--489.

[11] Wilson, W.R. D. (1991), Friction models for metal forming in the boundary lubrication regime, *Trans. ASME J. Eng. Mat.* Tech,, 113, 60--68.